Inter-Laboratory Study Protocol

Validation of Computational Solid Mechanics Models Using Full-Field Optical Data

Version 10th December 2013

Inter-laboratory Study Protocol

Validation of Computational Solid Mechanics Models Using Full-Field Optical Data

This protocol is based on the "A Guideline for the Validation of Computational Solid Mechanics Models Using Full-Field Optical Data" that wasprepared as part of the ADVISE project (Grant Agreement SCP7-GA-2008-218595) within the European Commission's Safety and Security by Design Programme (FP7-SST-2007-RTD-1).It has been adapted in the VANESSA Coordination and Support Action (Grant Agreement FP7-NMP-2012-CSA-6).

Cite as: 'ILS Protocol for the Validation of Computational Solid Mechanics Models Using Full-Field Optical Data', VANEESA, 2013.

Electronic copies can be downloaded at www.engineeringvalidation.org

Publisher: VANESSA Project Consortium

The partners in the VANESSA(**Validation of Numerical Engineering Simulations: Standardisation Actions**) project are: Centro Ricerche Fiat, Dantec Dynamics, EMPA Swiss Federal Laboratories for Materials Science and Technology, High Performance Space Structure Systems GmbH, National Nuclear Laboratories, SNV Swiss Association for Standardization, the University of Liverpool, and the Laboratory of Technology and Strength of Materials of University of Patras.

The following members of the project contributed to the many discussions which led to the production of this protocol:

Eann Patterson	University of Liverpool, UK (*Co-ordinator of VANESSA*)
Erwin Hack	EMPA, Swiss Federal Laboratories for Materials Science and Technology, Switzerland
Alexander Ihle	High Performance Space Structure Systems GmbH, Germany
George Lampeas	University of Patras - LTSM, Greece (VANESSA Task Leader for Validation ILS)
Andrea Pipino	Centro Ricerche Fiat, Italy
Paul Ramsey	National Nuclear Laboratory, UK
Hans Reinhard Schubach	Dantec Dynamics GmbH, Germany
Chris Sebastian	University of Liverpool, UK
Thorsten Siebert	Dantec Dynamics GmbH, Germany
Nassia Tselepi	National Nuclear Laboratory, UK
Rolf Widmer	SNV, Switzerland

CONTENTS

Executive Summary

Engineering simulation is an essential feature of the analysis and design of all engineered products at all scales. In particular, simulation based on computational solid mechanics models permits designers to optimise the load-bearing components in devices, machines and structures, such that a satisfactory level of reliability is achieved for an acceptable cost. The need for validation of computational solid mechanics models is becoming more important, particularly as new materials and complex structures provide severe challenges to reliable simulations. Validation procedures are required to provide the confidence in simulation models and assess the simulation uncertainty. These confidence levels should be acquired through rigorous, quantitative validation of the models employed for the simulations. Although many engineering companies and organisations have developed internal procedures for validating the computational models that are essential to their engineering design activities, such simulations are not routinely validated, at least in part, because a methodology for reliable, rapid and cost-effective validation had not been available, as well as because there are no standards for the validation of computational solid mechanics models used in engineering design. Consequently, many engineering artefacts are designed using inadequately validated models, which when this is recognised leads to conservative design and when it is not recognised leads to unreliable design.

The purpose of this document is to provide a protocol for an inter-laboratory study (ILS) to evaluate the effectiveness of a proposed methodology for the validation of computational solid mechanics simulation models using full-field optical measurements of strain and, or displacement. The process for validating models of structural components using full-field data from optical methods measurements is described in detail. Dimensionality of data fields derived by simulation or experimentation is reduced by the use of image decomposition based on feature vectors, which contain the coefficients of the shape descriptors, such as Fourier descriptors or orthogonal polynomials, employed to describe the data field. This approach enables a simple comparison of data-rich fields from a computational model and a validation experiment to be made utilising the uncertainty to assess the acceptability of the correlation.

The engineering community is invited to participate in the inter-laboratory study and to support this activity. An overview of the methodology for validation of computational solid mechanics models is provided in section 1. Participants in the ILS are provided with a choice of three exemplars, described in section 2, to which the validation methodology can be applied. These exemplars are: a thermomechanical analysis of an antenna reflector (data only available); a wedge indenter deforming a rubber block (data and specimens available), and the three-point bending of an I-beam with open holes in the web (data and specimens available).

In section3, the protocol for the step-by-step application of the validation process and the recording of results is provided. Displacement and / or strain plots in ‘tiff’ format are provided for use in the validation process. An image decomposition software package, which can be used for the image decomposition, together with an excel file for the visualization of the results are also provided.

1. Overview of Validation Methodology

The verification and validation of simulations conducted in computational solid mechanics has been identified as an essential step in the process of design analysis[1]. In this context validation has been defined as "the process of determining the degree to which a model is an accurate representation of the real world from the perspective of the intended uses of the model". A guideline for the validation of computational solid mechanics models using full-field optical data, was developed in the ADVISE project[2]with the aim of providing a framework for the validation of analysis and simulation of structural components. The process focuses on the quantitative comparison of data-rich maps of strain and / or displacement fields obtained from optical measurements with the respective results from a computational model. The acceptability of the comparison is discussed in the context of the uncertainties associated with the data from the model and the experiment, and with the comparison process.

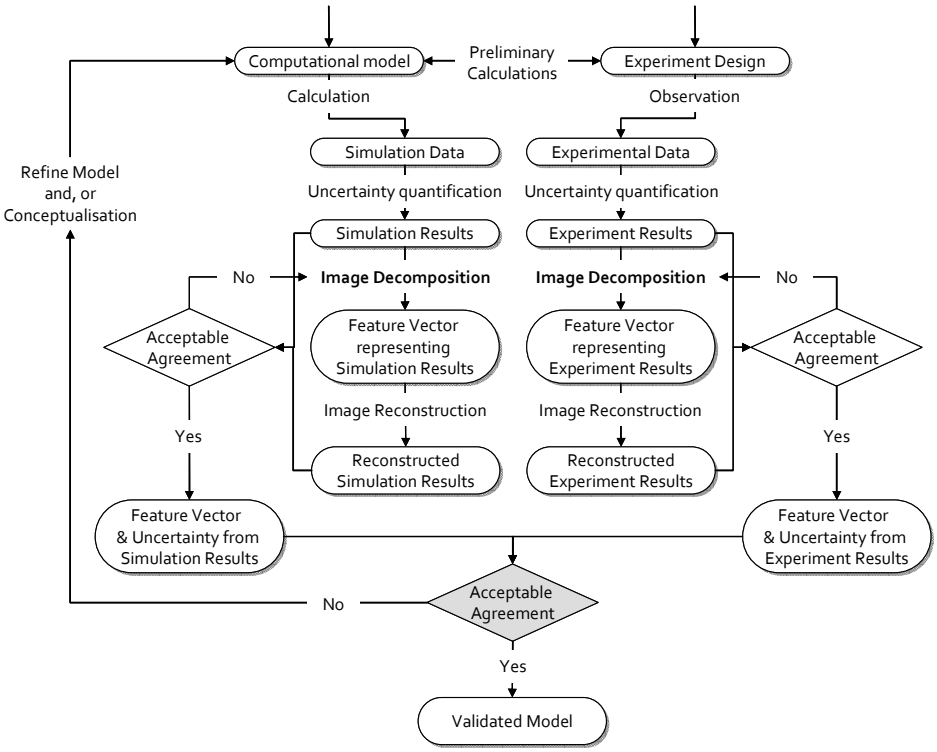

Figure 1.1: Flow chart of the validation methodology[3]

The validation methodology is schematically shown in figure 1.1. In brief, it consists of reducing the dimensionality of data fields from a matrix consisting of tens of thousands of values to a feature vector with, ideally between ten and

[1]ASME V&V 10-2006, *Guide for verification and validation in computational solid mechanics, American Society of Mechanical Engineers*, New York, 2006.
[2]ADVISE, 'Advanced Dynamic Validations using Integrated Simulation and Experimentation' ; a project that was supported by EU grant SCP7-GA-2008-218595 and MichiganStateUniversity.
[3]Sebastian, C., Hack, E., Patterson, E.A., 2013, An approach to the validation of computational solid mechanics models for strain analysis, *J. Strain Analysis*, 48(1):36-47.

twenty elements, using image decomposition based on e.g. orthogonal polynomials.

The accuracy with which the feature vector represents the original data is assessed for both the data fields from experiment and the model, after which the elements of the feature vectors representing the data from experiment and model are plotted as a function of one another. For a valid model, all of the points in the plot will fall within a zone on either side of the line of unit gradient with bandwidth defined by the uncertainty in the feature vectors representing the data from the experiment. More details about the validation methodology are provided in Appendix I of the present document.

2. Description of validation methodology demonstrators

A choice of three exemplars are provided for this inter-laboratory study with the aim of providing at least one that appeals to all potential participants. Participants may choose to consider one or more of the exemplars. The first exemplar, which has been provided by HPS GmbH, is available only as data sets from experiments and simulations performed by the company. This is for proprietary reasons but the exemplar provides real data from an industrial study.

The second exemplar is a simple geometry of a wedge-shaped indenter in contact with a rectangular rubber block. The problem becomes challenging as the depth of indentation is increased and the deformation becomes non-linear. Data from experiments and simulations performed at the University of Liverpool are available, but participants may also borrow an indenter and rubber block in order to perform the experiment and, or to construct a finite element model in order to generate their own data.

The third exemplar is an aluminium I-beam with open holes cut in the web, a common structural element in the aircraft industry (e.g. in wing spars), as well as in marine and civil engineering applications. The I-beam is subjected to three-point bending. Data from experiments and simulations performed by the University of Patras are available and participants may also borrow an I-beam and, or develop a finite element model in order to generate their own data.

2.1Thermomechanical analysis of an antenna reflector

2.1.1. Introduction

Under ESA contract N° 22377/09/NL/US ARTES 5.2 program, HPS GmbH has developed a multi-beam dual reflector antenna structure for high frequency radio communication satellites. Such antenna reflectors have to exhibit inherently very low thermo-mechanical deformations in the range of some 10 micro-meters over a large temperature range. Therefore, these types of antenna reflectors are almost exclusively made of ultra high modulus carbon fiber composites and are in most cases partly covered with multi-layer (MLI) insulation to protect them e.g. from the sun's radiation and IR earth albedo.

Figure 2.1: Full CFRP antenna reflector, partly covered with MLI

One of the challenging tasks in such developments is the thermo-mechanical modelling in terms of both deformation prediction and model correlation.

2.1.2 Finite Element Modelling and Testing

For in-orbit thermo-mechanical distortion prediction, a thermal and mechanical FE model has been established. This allows non-linear thermal analysis to be performed and the temperature distributions to be applied to the mechanical model. Eventually, the resulting full-field deformation of the antenna reflector is obtained.

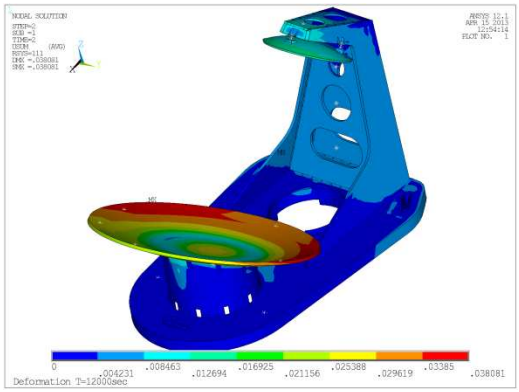

Figure 2.2: FE Model of the antenna (thermo-mechanical deformation plot)

To verify the performance of the antenna main reflector and to qualify/accept it for integration on a satellite, it has to undergo a comprehensive test campaign. One of these tests being a so-called thermal-vacuum-cycling test, is performed in a space simulation chamber to test the antenna's thermal and thermo-mechanical behavior in a vacuum and for different temperature stages typically ranging from -120 °C to +120 °C. During this test the resulting deformations of the antenna reflector are measured using, for example, an ESPI system; the minimum measurement uncertainty is 3um for out-of-plane displacements.

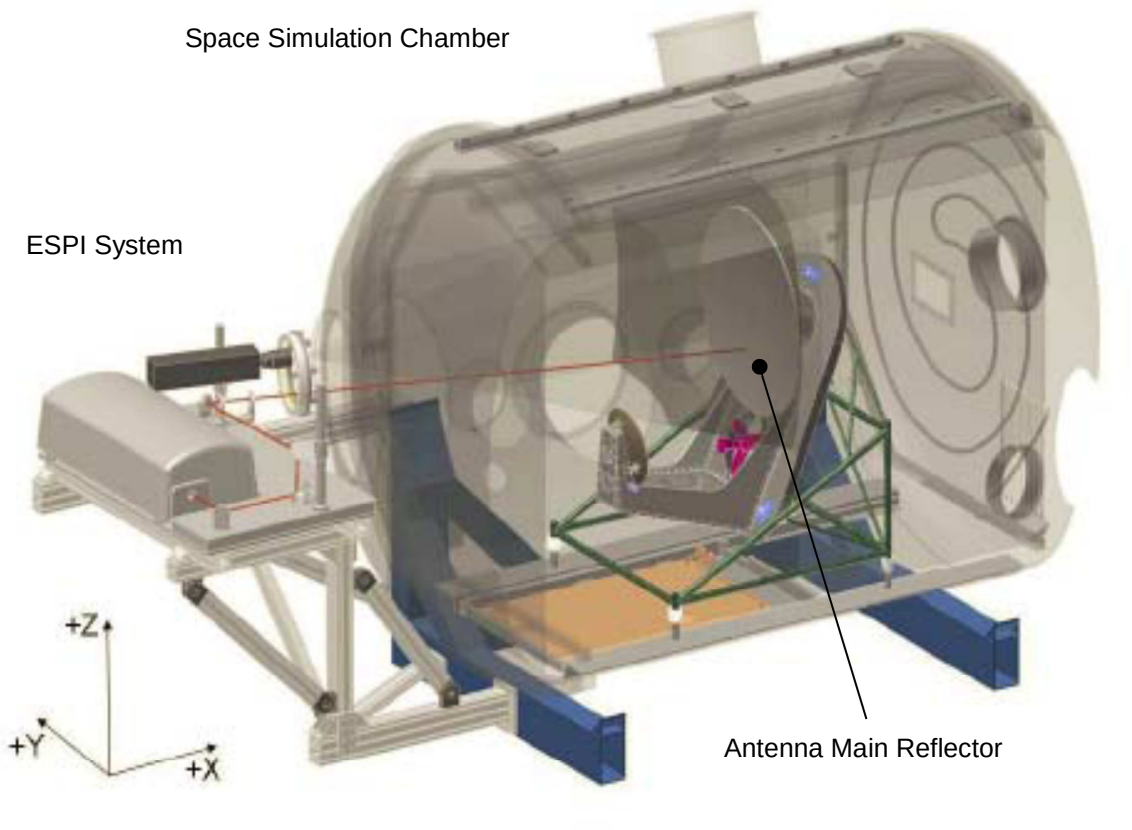

Figure 2.3: Thermal-vacuum-cycling test setup

2.1.3 Test Results and Model Correlation

From the ESPI system a deformation plot over the complete temperature range is acquired. Similar to these measured plots, full-field deformation data is also obtained from the FE model.

With the ESPI system data being in the range of 1.3 million data points, a quantitative model correlation using the full-field data is rather challenging in terms of data post-processing and comparison. Therefore, the common approach is to use selected lines through the data and to compare the measured and calculated results in a qualitative manner.

To update and correlate the FE model several simulation runs with different boundary conditions and model properties are performed and compared to the measured results along the selected lines, as shown in figures 2.4 and 2.5.

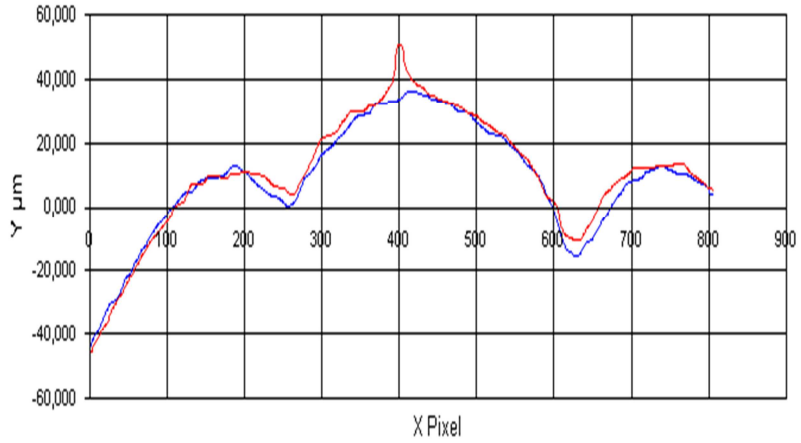

Figure 2.4: Two measured deformation line cuts after 4800sec of heating

The thickness of the adhesive was believed to be one of the critical parameters in this study and so it was modified in an attempt to improve the correlation between the results from the model and experiments. Some typical results from this parametric study are shown in Figure 2.5.

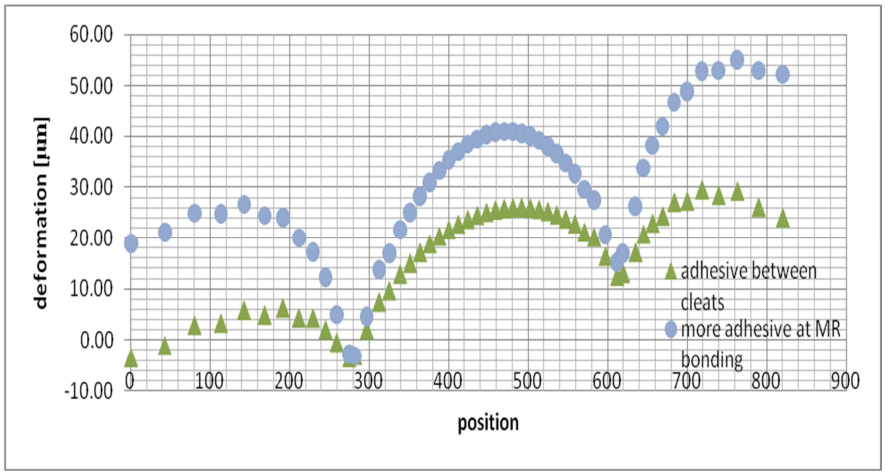

Figure 2.5: FEM simulation: deformation after 4800sec of heating (line cut)

2.1.4 Description of the Provided Data

For this case study, the component and its finite element model are not available to participants in the ILS due to their proprietary nature. However data from both experiments and simulations performed by HPS are available, as presented in figure 2.6.The data package for this test case contains the following surface plots:

- Measured out-of-plane deformation (**TVC-test_ESPI_measured.tif**),
- Out-of-plane deformation results of FE simulation variant 3 (**FE-simulation_var3.tif**), and
- Out-of-plane deformation results of FE simulation variant 7 (**FE-simulation_var7.tif**).

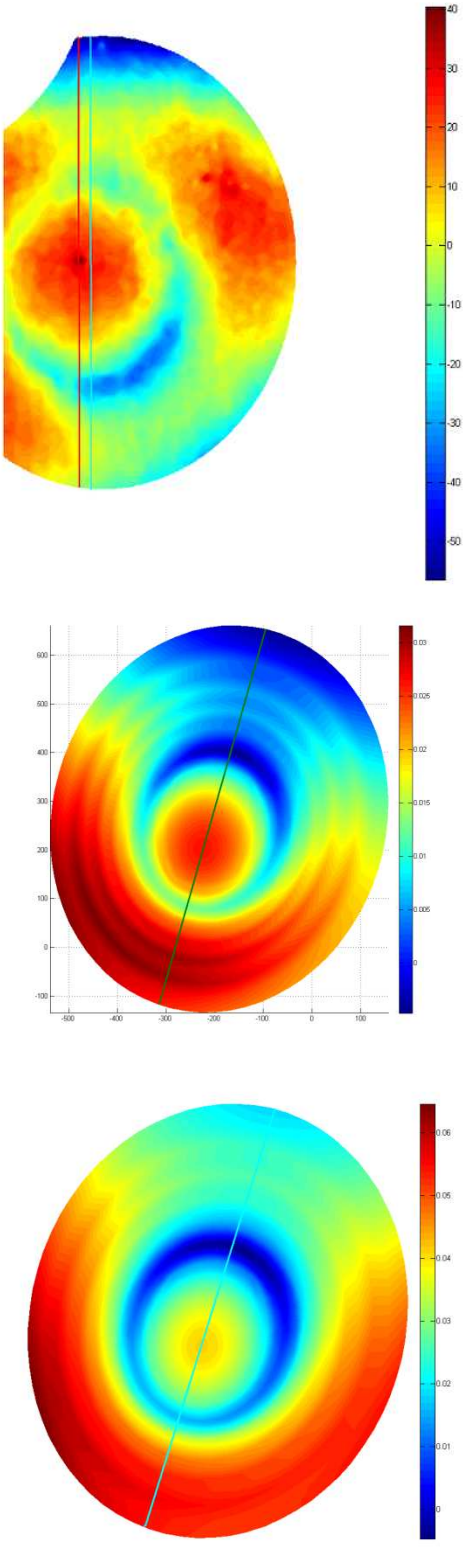

Figure 2.6: Test data (top), FE simulation variant 3 (center), FE simulation variant 7 (bottom) for the antenna reflector with the sections shown for which data are plotted in figures 2.4 and 2.5.

The deformations in the surface plots are represented by discrete colors (RGB), with minimum and maximum values provided in Table A. The scaling from minimum to maximum is linear.

Table A: Minimum and maximum values of data fields

Dataset id	**File including dataset (Measured field / Predicted field)**	**Measured displacement fields**		**Predicted displacement fields (FEM)**	
		Min. value	Max. value	Min. value	Max. value
1	TVC-test_ESPI_measured.tif / FE-simulation_var3.tif	-56.5 µm	40.4 µm	-4.7 µm	31.6 µm
2	TVC-test_ESPI_measured.tif / FE-simulation_var7.tif	-56.5 µm	40.4 µm	-4.7 µm	64.6 µm

2.2 Wedge indenter deforming a rubber block

2.2.1 Introduction

In this case study a rigid, wedge-shaped indenter was pressed onto an elastic, rectangular body. A numerical result for an elastic half-plane indented by a rigid wedge was given previously by Jayadevan and Narasimhan[4]. More recently, a good agreement between numerical and theoretical results was shown for the axi-symmetric frictionless indentation of an elastic layer on a rigid base by Jaffar[5]. It is difficult to obtain accurate analytical solutions for this kind of contact problem, so asymptotic methods are commonly implemented in theoretical analysis[6]. Since an indenter with a blunted apex is more applicable to real problems, Korsunsky illustrated the influence of small variations in punch shape on the contact behaviour for a blunted Hertzian indenter and a rounded cone[7]. Ciavarella and his co-workers have addressed elastic contact problems involving a blunted wedge and an elastically similar half-plane[8]. It can be seen that some progress has been made to resolve this engineering contact problem using analytical and numerical models, in which many of the following assumptions are commonly employed:

a) small strains within the elastic limit;
b) each body considered as an elastic half-plane, i.e., the area of contact is much smaller than the characteristic radius of the body;
c) there are no shearing tractions present, which requires the surfaces to be frictionless;
d) the contacting bodies are elastically similar; and
e) the external angle of the wedge is very small.

These simplifying assumptions will induce some deviation relative to the actual situation and the validation procedure described in this protocol has been applied to assess the extent of this deviation at various levels of indentation using data from digital image correlation[9]. It is proposed here to validate a finite element problem of the same contact scenario using data from digital image correlation.

2.2.2 Experimental Apparatus and Procedure

The experimental arrangement used in this study is shown schematically in figure 2.7. The specimen being indented was a rectangular block with dimensions 60mm×60mm×25mm, which was cured from a Room Temperature Vulcanization

[4]Jayadevan, K. R., Narasimhan, R., Finite-element simulation of wedge indentation. *Comp. &Struct.*57(5), 915-927, 1995.
[5]Jaffar, M. J., Frictionless contact between an elastic layer on a rigid base and a circular flat-ended punch with rounded edge or a conical punch with rounded tip.*Int. J. Mech. Sci.* 44(3), 545-560, 2002.
[6]Dini, D., Barber J. R., Churchman, C. M., Sackfield, A. and Hills, D. A., The application of asymptotic solutions to contact problems characterised by logarithmic singularities. *Eur. J. Mech. A-Solids* 27(5), 847-858, 2008.
[7]Korsunsky, A. M., The influence of punch blunting on the elastic indentation response. *J. Strain Anal. Eng. Des.*36(4), 391-400, 2001.
[8]Ciavarella, M., Hills D. A. &Monno, G., Contact problems for a wedge with rounded apex.*IJ.Mech. Sci.* 40(10), 977-988, 1998.
[9]Tan, X., Kang, Y., Patterson, E.A., A study of the contact of a rounded rigid indenter with a soft material block, *J. Strain Anal*., in press, 2013.

(RTV) rubber (106RTV, Hongxitai Company, China; also available from ACC Silicones, UK). It was cast into an aluminium mould following the instructions supplied with the material and then removed from the mould before curing at room temperature for 24 hours. After curing, a very thin coat of quick-drying white paint (Matt Super White 1107, Plasti-kote, UK) was sprayed onto one of the square (60mm×60mm) surfaces using an aerosol can followed by a very fine dusting of black speckle (Matt Super Black 1102, Plasti-kote, UK) on top of the white paint. During the experiment, the surface deformation of the specimen was deduced from the displacement of the randomly distributed small paint dots using digital image correlation.

A wedge-shaped indenter with a slope angle of 73.5 degrees was manufactured from 2024 Aluminum alloy with a tip radius, R=1.68mm and a thickness of 25mm, which was the same as the rubber specimen. Care was taken to ensure that the specimen was not pre-stressed and it was placed in the centre of an aluminum disc (diameter of 108mm and thickness of 8mm) which was mounted in the bottom grip of an electric-drive loading machine (Electropuls E1000, Instron, High Wycombe, Buckinghamshire), while the indenter was mounted in the top grip of the machine. A three-dimensional digital image correlation system (Q-400, Dantec Dynamics GmbH, Germany), consisting of two cameras (FireWire, 1/8", 1624×1234 pixel) fitted with lenses of focal length of 50mm, which gave a magnification of 35pixels/mm, was used to acquire data. Two green LED light sources were positioned approximately 30 cm in front of the painted surface of the specimen. The control software (Bluehill, Instron, UK) for the loading machine was set to apply load at a constant rate of 1 mm/min, and the DIC software (ISTRA 4D) was programmed to record specimen images every 30 seconds. The surfaces in contact were dry, i.e. there was no lubricant introduced. In-plane calibration procedures were conducted in order to provide confidence in the measured results and to establish the minimum measurement uncertainty (0.0026ε, 0.0105ε, 0.0135ε and 0.0243ε for 2mm, 4mm, 6mm and 9mm loading cases respectively). Note that for data from the experiments, the strains were calculated from the displacements using the following expressions, which include the second order terms:

$$\varepsilon_{xx} = \frac{\partial u}{\partial x} + \frac{1}{2}\left[\left(\frac{\partial u}{\partial x}\right)^2 + \left(\frac{\partial v}{\partial x}\right)^2\right]$$
$$\varepsilon_{yy} = \frac{\partial v}{\partial y} + \frac{1}{2}\left[\left(\frac{\partial u}{\partial y}\right)^2 + \left(\frac{\partial v}{\partial y}\right)^2\right] \qquad (2.1)$$
$$\gamma_{xy} = 2\varepsilon_{xy} = \frac{\partial v}{\partial x} + \frac{\partial u}{\partial y} + \frac{\partial u}{\partial x}\frac{\partial u}{\partial y} + \frac{\partial v}{\partial x}\frac{\partial v}{\partial y}$$

The finite element model was created using the Abaqus 6.11 software package. The rubber block was modelled using 13,500 C3D8RH elements, which are 8-node linear hybrid elements. The rubber was assumed to be a hyperelastic material that could be described in terms of a strain energy potential, $U(\varepsilon)$. The Ogden stress-

deformation function[10] in the form of the Yeoh potential[11] was found to providethe optimum strain energy potential based on typical experimental stress-strain data[12,13]. The Yeoh potential was implemented in Abaqus using the following coefficients: N=3,D_1=9.90, D_2=-1.36, D_3=4.78, , α_1=1.54, α_2=5.84, α_3=-1.83, μ_1=0.37, μ_2=6.56 and μ_3=1.70.

The wedge was modelled as a discrete rigid part using 25,935 R3D4 elements, which are 4-node 3-D bilinear rigid quadrilateral elements.

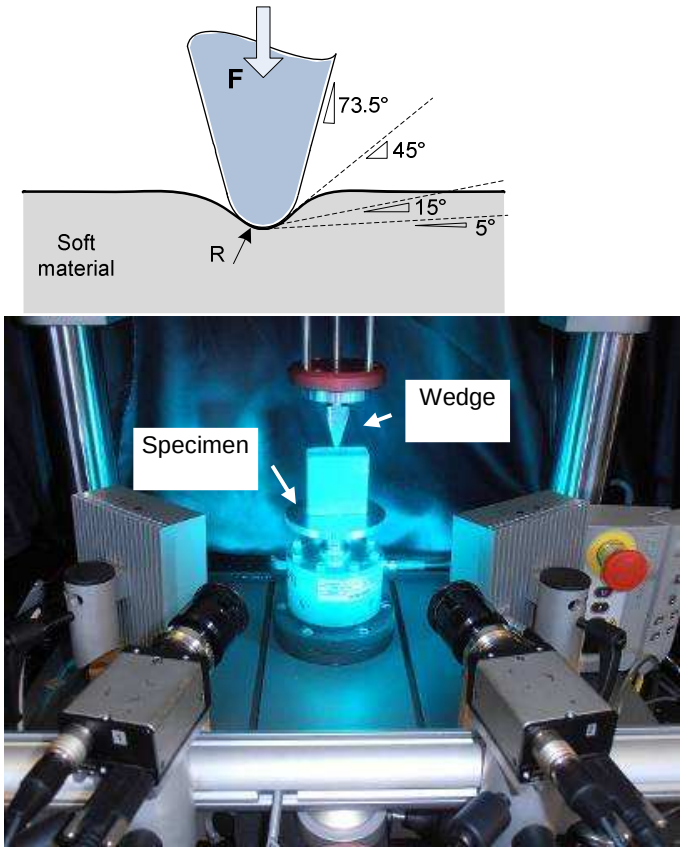

Figure 2.7: The experimental arrangements shown as a schematic (*left*) and photograph (*right*).

2.3.3 Description of the provided data

A pair of strain fields measured using DIC and predicted using the finite element model are shown in figure 2.8.

[10]Twizell, E.H., and Ogden, R.W., Non-linear optimisation of the material constants in Ogden's stress-deformation function for incompressible isotropic elastic materials, *J. Austral. Math. Soc. Ser. B*, 24:424-434, 1983.

[11]Yeoh, O.H., Some forms of the strain energy function for rubber, *Rubber Chemistry & Technology*, 66:754-771, 1993.

[12] Adams, L.H., Gibson, R.E., The compressibility of rubber, *Rubber Chemistry and Technology*, 3(4):555-562, 1930.

[13] Bridgman, P.W., The compression of twenty-one Halogen compounds and eleven other simple substances to 100,000 kg.cm3, *Proc. Am. Acad. Arts Sci*. 76(1):1-7, 1945.

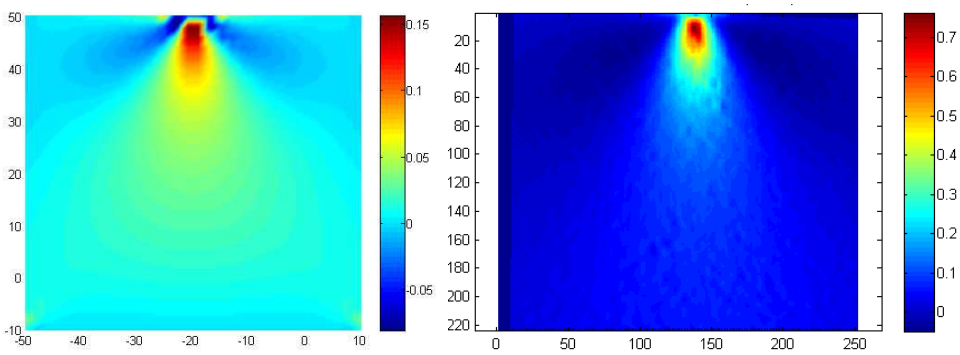

Figure 2.8: The predicted in-plane strain, ε_{xx} (*left*) and the corresponding field obtained using digital image correlation (*right*) for the rubber block subject to an indentation of 4mm.

The data package for this test case contains the following surface plots:

- Measured strain, ε_{xx} for indentation of δmm (measured_Exx-δmm.tif)
- Measured strain, ε_{yy} for indentation of δmm (measured_Exx-δmm.tif)
- Measured strain, ε_{xy} for indentation of δmm (measured_Exy-δmm.tif)
- Predicted strain, ε_{xx} for indentation of δmm (predicted_Exy-δmm.tif)
- Predicted strain, ε_{yy} for indentation of δmm (predicted_Exy-δmm.tif)
- Predicted strain, ε_{xy} for indentation of δmm (predicted_Exy-δmm.tif)

The δ value in each file name indicates the depth of indentation in each loading case and four cases are provided, namely 2, 4, 6 and 9mm. The deformations in the surface plots are given by discrete colors (RGB). The minimum and maximum values are given in Table B and the scaling between them is linear.

Table B: Minimum and maximum values of data fields

Dataset id	Dataset content	Measured strain fields (unit strain)		Predicted strain fields(unit strain)	
		Min. value	Max. value	Min. value	Max. value
3	measured_Exx-2mm.tif/predicted_Exx-2mm.tif	-0.0167	0.1847	-0.0516	0.0858
4	measured_Eyy-2mm.tif/predicted_Eyy-2mm.tif	-0.1703	0.0247	-0.160	0.0585
5	measured_Exy-2mm.tif/predicted_Exy-2mm.tif	-0.1696	0.1632	-0.102	0.102
6	measured_Exx-4mm.tif/predicted_Exx-4mm.tif	-0.049	0.762	-0.091	0.158
7	measured_Eyy-4mm.tif/predicted_Eyy-4mm.tif	-0.6225	0.095	-0.329	0.125
8	measured_Exy-4mm.tif/predicted_Exy-4mm.tif	-0.5708	0.5379	-0.224	0.224
9	measured_Exx-6mm.tif/predicted_Exx-6mm.tif	-0.0808	0.9615	-0.150	0.215
10	measured_Eyy-6mm.tif/predicted_Eyy-6mm.tif	-0.7398	0.1277	-0.463	0.136
11	measured_Exy-6mm.tif/predicted_Exy-6mm.tif	-0.6888	0.629	-0.341	0.341
12	measured_Exx-9mm.tif/predicted_Exx-9mm.tif	-0.4984	1.3733	-0.178	0.287
13	measured_Eyy-9mm.tif/predicted_Eyy-9mm.tif	-0.998	0.3429	-0.523	0.0862
14	measured_Exy-9mm.tif/predicted_Exy-9mm.tif	-1.0048	0.9065	-0.519	0.515

2.3 Three-point bending of an I-beam with open holes

2.3.1. **Introduction**

An I-beam with holes in the web is a common structural element in the aircraft industry (e.g. in wing spars), as well as in marine and civil engineering applications. The I-beam considered here is made from Aluminium alloy 6060, has 500mm length, while its cross section has 65mm web height, 42.5mm flange widthanda uniform thickness of 2.5 mm. In the beam web,open holes of diameter 35mmwere drilled at a pitch distance of 100mm.

The I-beam was loaded in an MTS hydraulic machine under three-point bending, at a constant rate of 1 mm/min. The loadwas applied in the middle of the top flangeusing a roller of 60mmdiameter, while the beam was supported underthe lower flange on two rollers of 50mm diameter, which were placed symmetrically about the beam central cross-section at a distance of 450mm.

A schematic diagram of the I-beam, as supported and loaded, is shown in figure 2.9.

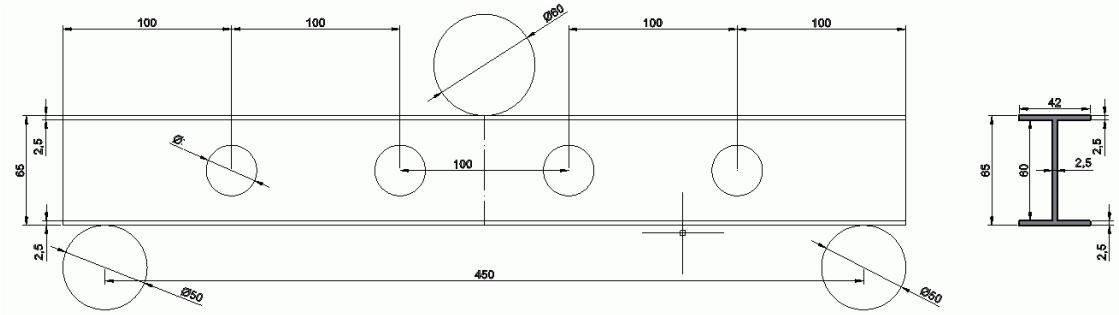

Figure 2.9: Schematic diagramof the I-beam with holes

2.3.2 Finite Element Modelling and Testing

For the simulation of the three-point bending test, a mechanical FE model has been developed; the FE mesh of the model is shown in figure 2.10. The FE model allows both linear and non-linear structural analysis to be performed and the resulting full-field displacement / strain distributions to be calculated. The commercial code Ansys has been used in the model development. The selected element type for the analysis was the shell 181, which is a 4-node element with six degrees of freedom at each node and it is suitable for analyzing thin to moderately-thick shell structures. The material was modelled by an elastoplastic material model with kinematic hardening.

To validate the I-beam simulation model, full-field displacement and strain data have been acquired during the test using a DIC system. A three-dimensional digital image correlation system (Aramis 5M), consisting of two cameras (2448 x 2050 pixel) was used to acquire data.

The minimum measurement uncertainty is calculated to be 30με for in-plane strain and 10μm for in-plane displacements.

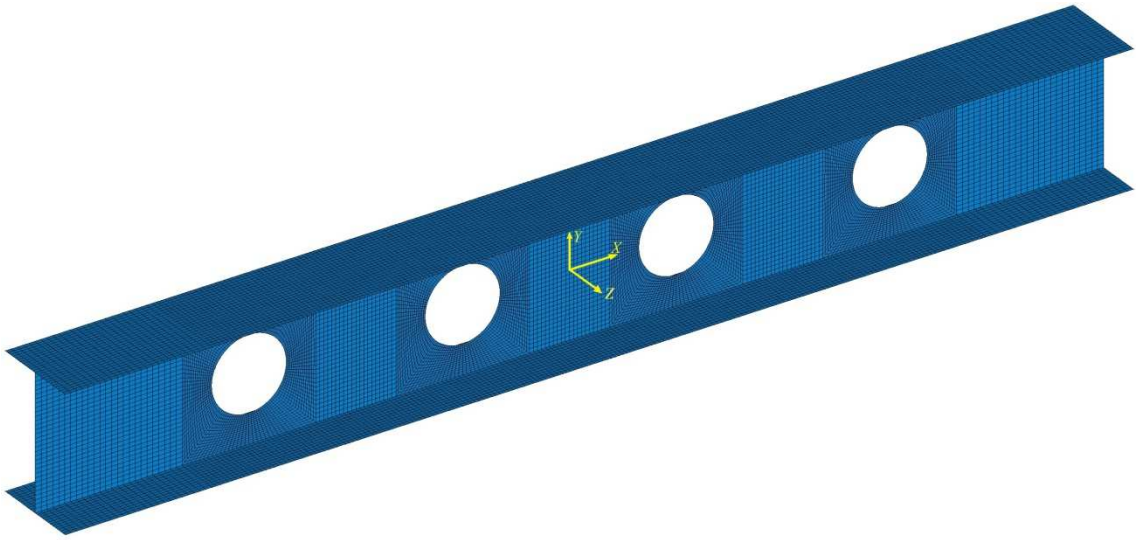

Figure 2.10: FE mesh of the I-beam simulation model

2.3.3 **Test Results and Model Correlation**

Displacement and strain plots from DIC and FE for the area around the two middle open holes are provided in figures 2.11 and 2.12, for an applied load of 9.8 kN.

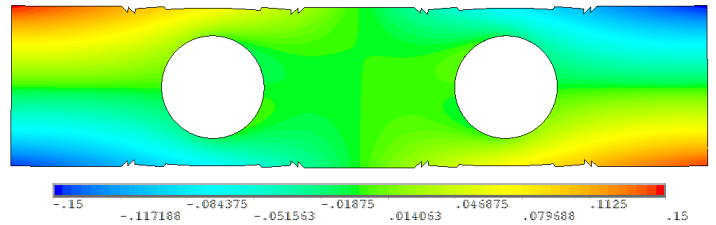

(a)

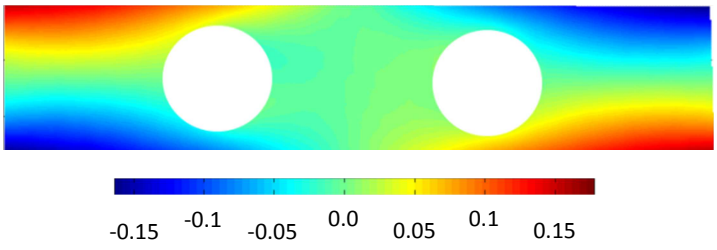

(b)

Figure 2.11:Displacement(mm) in the x-direction from(a) simulation model and (b) DIC

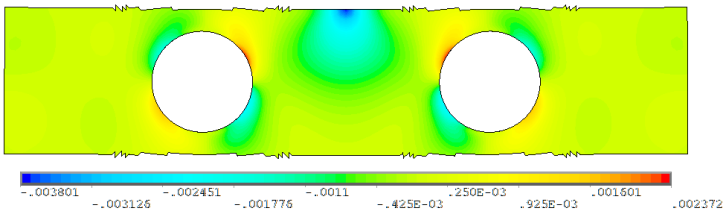

(a)strain (-)

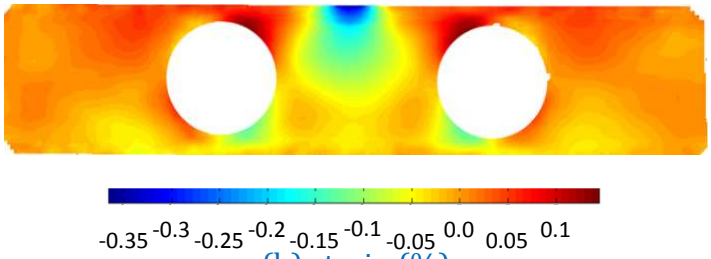

(b) strain (%)

Figure 2.12:Surface strains in the y-direction from (a) simulation model and (b) DIC

2.3.4 **Description of the Provided Data**

The data package for the I-beam case is presented in Table C.The displacements / strains in the surface plots are represented by discrete colors (RGB), with linear scaling from the minimum to maximum values, which are provided in Table C for each case.

Table C: Minimum and maximum values of data fields

Data set id	File including dataset (Measured field / Predicted field)	Measured fields (DIC)		Predicted fields (FEM)	
		Min. value	Max. value	Min. value	Max. value
15	DIC/FEM_ux-middle.tif	-0.0498mm	0.0413mm	-0.044mm	0.044mm
16	DIC/FEM_uy-middle.tif	0.0248mm	0.1538mm	0.046mm	0.1538mm
17	DIC/FEM_ex-middle.tif	-1209uε	1343uε	-1722uε	1323uε
18	DIC/FEM_ey-middle.tif	-3650uε	757uε	-4790uε	856uε
19	DIC/FEM_ux-side.tif	-0.1455mm	0.141mm	-0.1266mm	0.1486mm
20	DIC/FEM_uy-side.tif	0.3766mm	0.7035mm	0.4103mm	0.7133mm
21	DIC/FEM_ex-side.tif	-1439uε	1372uε	-1539uε	1509uε
22	DIC/FEM_ey-side.tif	-625uε	622uε	-797uε	830uε

3. Validation Protocol

3.1 General data (reference to protocol Table 1):

Select one of the exemplars from section 2and note down the case selected.

In cases where resources other than those provided were used, please describe them briefly in Table 1, including information about simulation software, experimental testing, shape descriptor software and any other resources used for the validation process. Note that measurements need to be acquired with an instrument for which the calibration uncertainty has been quantified.

Table 1: General data		
Your comments:	Participant data (optional)	
	name / email address:	
	organization / department :	
	position on the organization / main role	
	date	
	Validation exemplar selected (2.1, 2.2 or 2.3) *(*) in case of a user selected exemplar, please insert a sketch or short description*	
	Resources used *(optional - to be filled only in case resources other than those provided were used)*	
	simulation software used	
	experimental test performed, machine used, DIC used	
	shape descriptor decomposition softwareused	
	other resources description	

3.2 Feature vectors calculation (reference to protocol Table 2)

While, the proportion of the surface area of the artifact over which data fields should be validated will depend on the purpose for which it is intended to employ the model; it is recommended that data should be acquired from the entire surface of a component to which optical access can be achieved. The surface may be sub-divided to avoid obstructions to optical access, to achieve pseudo-planar conditions in the field of view, and to ensure sufficient spatial resolution. The latter two factors are important in reducing measurement uncertainties. In Table 2 record the dataset id, as well as information about the region of interest (ROI) from which data has been acquired in the experiment.

In general, computational solid mechanics models intended for use in predicting structural integrity should be validated using full-field maps of strain. However, in some cases, displacement maps are also of high importance. Select the component of strain or displacement to be used for validation purposes and record it in Table 2.

Insert in the table the images of the original data fields for the ROI from both the experiment and simulation.

Decompose the two data fields using the software provided, or otherwise, to generate a pair of feature vectors which are invariant to scale, translation and rotation. This invariance allows comparison of data fields to be made using their representative feature vectors regardless of whether the fields are in the same coordinate system, have the same spatial scale, orientation, or sampling grid. The only consideration is that the fields should share a common ROI relative to the artifact.

When using the software provided, a decision on the type of polynomial, e.g. Tchebichef or Krawtchouk, used in the decomposition process will need to be made and recorded in Table 2.

For instance using Tchebichef polynomials, $T(i, j)$, up to the order N,the datafield, $I(i, j)$ can be decomposed as a series expansion of

$$I(i, j) = \sum_{k=0}^{N} s_k T_k(i, j) \qquad (1)$$

in which the coefficients s_k constitute the feature vector and are given by

$$s_k = \sum_{i, j}^{n} I(i, j) T_k(i, j) \qquad (2)$$

where$n$ is the number of data points. Since the polynomials are dimensionless, all s_k have the same unit as the data field$I$. The identity Eq.(1) is exactly valid for $N=\infty$ or $N=n$. However, it has been found that no advantage is gained by using a series expansion of order greater than twenty and that eight is usually sufficient.

Record the values of the Nshape descriptors s_k used in the decomposition of both the data from experiment and simulation.

The number of shape descriptors, N, can be limited by considering the accuracy with which the feature vector describes the original field by reconstructing the

strain / displacement field from the feature vectorand assessing the average reconstruction residual:

$$u^2 = \frac{1}{n}\sum_{i,j}^{n}\left(\hat{I}(i,j) - I(i,j)\right)^2 \qquad (3)$$

where $\hat{I}(i,j)$ is the reconstructed value of *I(i, j)*which is the original data; and the average residual, u should be no greater than the minimum measurement uncertainty, obtained from the calibration of the measurement instrument[14,15]. In addition, no location should show a clustering of residuals greater than $3u$, where a cluster is defined as a group of adjacent pixels comprising 0.3% or more of the total of number of pixels $n$in the region of interest. If these requirements are not achieved then the number of elements in the feature vector could be increased or a different set of shape descriptors could be employed, e.g. Krawtchouk instead of Tchebichef.The same method and convergence criteria should be applied for the decomposition of both experimental and simulation data.

Record the average reconstruction residual in Table 2 for both the data from the experiment, $u_{E,}$ and simulation, $u_{M,}$.

Insert in Table 2 plots from the reconstructed data fields from the experiment and simulation model.

[14]Sebastian, C., Patterson, E.A., 2013, Calibration of a digital image correlation system, *Experimental Techniques*, doi. 10.1111/ext.12005

[15]Whelan, M.P., Albrecht, D., Hack, E., Patterson, E.A., 2008, 'Calibration of a speckle interferometry full-field strain measurement system', *Strain*, 44(2):180-190.

<table>
<tr><td>Table 2: Feature vectors calculation</td><td colspan="3">Record the dataset id</td></tr>
<tr><td>Your comments:</td><td colspan="3">Record information about the region of interest (ROI)</td></tr>
<tr><td>Your comments:</td><td colspan="3">Record the component of strain / displacement used</td></tr>
<tr><td>Your comments:</td><td colspan="2">Insert original data plot from experiment</td><td>Insert original data plot from model</td></tr>
<tr><td>Your comments:</td><td colspan="3">Insert type of polynomial usedin decomposition (e.g. Tchebichef or Krawtchouk)</td></tr>
<tr><td>Your comments:</td><td colspan="3">Record the average reconstruction residual for the data from the experiment , u_E</td></tr>
<tr><td>Your comments:</td><td colspan="3">Record the average reconstruction residual for the data from the simulation, u_M</td></tr>
<tr><td rowspan="10">Your comments:</td><td>Shape descriptor</td><td>Shape descriptor from exp.</td><td>Shape descriptor from model</td></tr>
<tr><td>1</td><td></td><td></td></tr>
<tr><td>2</td><td></td><td></td></tr>
<tr><td>3</td><td></td><td></td></tr>
<tr><td>4</td><td></td><td></td></tr>
<tr><td>5</td><td></td><td></td></tr>
<tr><td>6</td><td></td><td></td></tr>
<tr><td>.</td><td></td><td></td></tr>
<tr><td>N</td><td></td><td></td></tr>
<tr><td>Your comments:</td><td></td><td>Insert reconstructed plot from experiment</td><td>Insert reconstructed plot from model</td></tr>
</table>

(for additional comparisons, e.g. another dataset, another ROI or another magnitude of strain / displacement, please add additional tables)

3.3 Uncertainty calculation (reference to protocol Table 3)

The experiment should have been performed using an instrument that had been calibrated in a manner that allows the calibration uncertainty to be evaluated and used as the instrument's minimum measurement uncertainty.

Record the dataset id in Table 3.Record the calibration uncertainty $u_{cal}(\varepsilon)$ for the instrument used to acquire the strain data in the experiment.

The total uncertainty in the feature vector describing the data from the experiment $u(s_E)$, should be calculated using the average reconstruction residual from the decomposition process described above, u_E and the calibration uncertainty:

$$u(s_E) = \sqrt{u_{cal}^2(\varepsilon) + u_E^2} \qquad (4)$$

Record the value of $u(s_E)$ in Table 3.

Table 3: Uncertainty calculation	Record the dataset id	
Your comments:	$u_{cal}(\varepsilon)$	
	u_E	
	$u(s_E)$	

(for additional comparisons, e.g. another dataset, another ROI or another magnitude of strain / displacement, please add additional tables)

3.4 Comparison of simulation and experimental data (reference to protocol Table 4)

Use the Excel file provided, or otherwise, to plot all N elements of the model feature vector (representing the strain or displacement data from simulation)against the experiment feature vector. The model can be considered to be a good representation of the reality of the experiment, if all of the plotted points lie within a band of width $\pm 2u(s_E)$ around the ideal line, $s_M = s_E$, where s_M and s_E are the terms in the feature vectors representing the strain fields from the model and experiment respectively.

Record the dataset id in Table 4.Insert the comparison plot (should look as the plot of fig. A-1, page 34) in table 4 and check whether or not the plotted points fall within the band defined above.

Make comments with respect to the acceptability of the results from the simulation, and hence the model.

<table>
<tr><td rowspan="5">Table 4: Comparison of simulation and experimental data

Your comments:</td><td colspan="2">Record the dataset id</td></tr>
<tr><td colspan="2">Excel plot of model versus experiment shape descriptors</td></tr>
<tr><td>Is model acceptable?</td><td></td></tr>
<tr><td></td><td></td></tr>
<tr><td></td><td></td></tr>
</table>

(for additional comparisons, e.g. another dataset, another ROI or another magnitude of strain / displacement, please add additional tables)

3.5 Validation methodology feedback (reference to protocol Table 5)

In Table 5,make general and specific comments about the validation procedure of this protocol, including information about your experiences, e.g. issues raised during the validation procedure, applicability of the validation procedure in your simulation cases, propose modifications in the methodology to cover your needs, ideas for improvement, any other comments.

Table 5: Validation methodology feedback	
Your comments:	

Please return the completed proforma and the files of your data fields to:

George Lampeas
Associate Professor
Laboratory of Technology and Strength of Materials,
Department of Mechanical Engineering and Aeronautics,
University of Patras,
26500 Rion, Patras, Greece
tel. no. 30 2610969498

labeas@mech.upatras.gr

Appendix I - Description of Validation Methodology

Data Acquisition

In many areas, it has been common practice to validate computational solid mechanics models using data from a single strain gauge or a set of strain gauges located in the region of maximum stress predicted by the model. This is simple and low in cost, but leaves results from the model not validated for the majority of the spatial domain with the possibility that, despite agreement at the location of the strain gauge, another larger stress is present elsewhere in the prototype and not predicted by the model. It also exposes a risk associated with removing material from the design in areas of predicted low or zero stress in order to save weight. Consequently, it is recommended that *validation of computational solid mechanics models, intended for use in predicting structural integrity, should be performed using full-field maps of surface strain and / or displacement.*

The advent of full-field methods of strain / displacement evaluation, utilizing non-contact optical techniques based on digital technology, provides the opportunity for a more comprehensive approach to be taken to the validation of computational solid mechanics models. Now, it is relatively easy and cheap to obtain deformation fields defined over the entire surface of engineering artefacts, by using techniques such as digital image correlation (DIC), digital speckle pattern interferometry (DSPI) and thermoelastic stress analysis (TSA). These techniques can be used to generate data-rich fields of displacement / strain that might contain of the order of 10^6 data points, which is comparable to the number of individual elements in a finite element model. Thus, in experiments, it is feasible to acquire data over the entire surface of an artefact; and, such a data field should provide the very strong evidence for validating a computational solid mechanics model. The data should be acquired using a calibrated instrument with a sufficiently low calibration uncertainty. However, in practice the surface may need to be sub-divided: to avoid obstructions to optical access; to achieve pseudo-planar conditions in the field of view; and to ensure sufficient spatial resolution. The latter two factors are important in reducing measurement uncertainties. While, the proportion of the surface area of the artefact over which data should be validated will depend on the purpose for which it is intended to employ the model; it is recommended that *data should be acquired from the entire surface to which optical access can be achieved and that the surface be sub-divided as necessary to reduce measurement uncertainties.*

The restriction to surface strain / displacement is appropriate because of the lack of readily-available techniques for measuring strain / displacement in the interior of an engineering artefact. Noting that techniques such as three-dimensional photoelasticity are only applicable to transparent materials and otherwise require models, and x-ray computed tomography is limited by its cost and the size of the object that can be examined.

It is good practice to conduct experiments specially designed for the purpose of generating data for a validation process. An experiment can be considered as a physical model of reality since usually it contains some level of idealisation in order to render it practical to conduct. The level of idealisation should be reduced to a minimum through the use of prototypes that come as close as possible to the

manufactured artefact in terms of geometry, material and scale; and should be used with loading and boundary conditions that reproduce those strain / displacement levels anticipated in service. There are many texts covering the topic of the design of experiments that can be consulted.

Image Decomposition

In general, strain / displacement fields obtained from experiments and computational models will be data-rich, i.e. containing data at more than 10^4 points, will be defined in different co-ordinate systems and in arrays with different pitches, and will be orientated differently, for instance, as a result of the location of the sensor in the experiment. These factors render the direct comparison of two strain / displacement fields impractical on a point-by-point basis. A practical alternative is to consider these fields as images in which the level of the strain / displacement is represented by the grey level values of the image. Then, these images can be decomposed to feature vectors containing typically less than 10^2 shape descriptors; and, a quantitative comparison made of the feature vectors. Typically, shape descriptors are the coefficients of orthogonal polynomials used to describe the image; and thus, for a specified set of appropriate polynomials, contain the information required to describe uniquely the essential features of the image.

The next section describes the process for making such a quantitative comparison. The remainder of this section describes a recommended process for strain / displacement field decomposition, assuming the engineering artefact is planar, or near to planar, in the region of interest (ROI); so that the effects of three-dimensional shape and perspective on the view are neglected.

The selection of an appropriate decomposition process for data fields can generate a set of shape descriptors that are invariant to scale, rotation and translation. This invariance allows comparison of strain / displacement fields to be made using their representative shape descriptors regardless of whether the fields are in the same coordinate system, have the same scale, orientation, or sampling grid. The only consideration is that the fields should share a common region of interest relative to the artefact.

Orthogonal shape descriptors possess the required invariance to scale, rotation and translation. Zernike, Tchebichef and Krawtchouk polynomials give rise to orthogonal shape descriptors. Zernike polynomials have been used to generate shape descriptors for modal shapes in vibration analysis and can also be used to represent strain distributions. However, they are based on a polar co-ordinate system and so are especially appropriate for fields with rotational symmetry. Tchebichef and Krawtchouk polynomials are defined on a Cartesian coordinate system and are discrete, so that they are an order of magnitude faster to implement for strain / displacement fields acquired from most optical systems. Zernike and Tchebichef polynomials yield global shape descriptors, and it has been found that they do not provide an accurate description of strain / displacement fields when there are cut-outs or holes due to the geometry of the artefact present in the image. This issue can be handled by tailoring the Zernike moments to the individual geometry; or using Krawtchouk polynomials; or by performing a fast

Fourier transform on the image and then representing the magnitude component of the FFT using either Zernike or Tchebichef polynomials.

The strain / displacement image, *I(i, j)* can be decomposed as a series expansion of Tchebichef polynomials, *T(i, j)*

$$I(i,j) = \sum_{k=0}^{N} s_k T_k(i,j) \qquad \text{(A1)}$$

in which the coefficients s_k constitute the feature vector and are given by

$$s_k = \sum_{i,j}^{n} I(i,j) T_k(i,j) \qquad \text{(A2)}$$

Note that since the polynomials are dimensionless, all s_k have the same unit as the image *I*, i.e. strain or displacement. The identity Eq.(A1) is exactly valid for $N=\infty$ or $N=n$ where *n* is the number of data points. However, it has been found that no advantage is gained by using a series expansion of order greater than twenty and that eight is usually sufficient. The number of shape descriptors, *N*, can be limited by considering the accuracy with which the feature vector describes the original field by reconstructing the strain / displacement field from the feature vector.

The goodness of fit of the reconstruction of a strain field to the original strain / displacement field should be assessed using the average squared residual

$$u^2 = \frac{1}{n} \sum_{i,j}^{n} \left(\hat{I}(i,j) - I(i,j) \right)^2 \qquad \text{(A3)}$$

where $\hat{I}(i,j)$ is the reconstructed value of I(i, j); and the average residual, *u* should be no greater than the minimum measurement uncertainty, obtained from the calibration of the measurement instrument. In addition, no location should show a clustering of residuals greater than 3*u*, where a cluster is defined as a group of adjacent pixels comprising 0.3% or more of the total of number of pixels in the region of interest.

If the reconstruction is found to be unacceptable, then steps should be taken to refine it until it becomes acceptable, and these may include employing a Fourier transform as described above, increasing the order of polynomial representation, selection of an alternative orthogonal shape descriptor, or tailoring of a shape descriptor.

The process of representing the data field by a set of shape descriptors is performed independently for the results from the model to be validated and from the experiment performed for the purpose of validation, but the identical type and order of shape descriptors must be used, resulting in two feature vectors $(s_E)_k$ and $(s_M)_k$, respectively. The goodness of the representation is described by the residual *u*, defined in equation (A3), which at the same time constitutes the uncertainty $u(s_k)$ of the shape descriptors, s_k. Since the image decomposition is made using orthonormal polynomials, this uncertainty is equal for all $k=1…N$.

Correlation of strain / displacement Fields

The shape descriptors representing the strain / displacement fields, for identical regions of interest, obtained from the model being validated and the experiment performed for the purpose of validation need to be compared quantitatively. It is recommended that the coefficients (elements of the feature vector) representing the results from the model should be plotted as a function of those obtained from the experiment. If the correlation was perfect then all of the resultant data points would lie exactly on a straight line of a gradient of unity. In practice, this will not occur either due to noise in the data or because the model is a poor representation of the reality of the experiment. The *model can be considered to be a good representation of the reality of the experiment, if all of the data-points lie within a band of width* $\pm 2u(s_E)$ *around the ideal line,* $s_M = s_E$ *(see Fig. A-1), where* s_M *and* s_E *are the shape descriptors representing the strain fields from the model and experiment respectively; and* $u(s_E)$ *is the uncertainty in the feature vector describing the data from the experiment and should be cited when describing the validity of the model.*

The experimental uncertainty is estimated from the residuals u_E, using equation (A3), but must be combined with the calibration uncertainty (given by equation (A6)), i.e.

$$u(s_E) = \sqrt{u_{cal}^2(\varepsilon) + u_E^2} \qquad \text{(A4)}$$

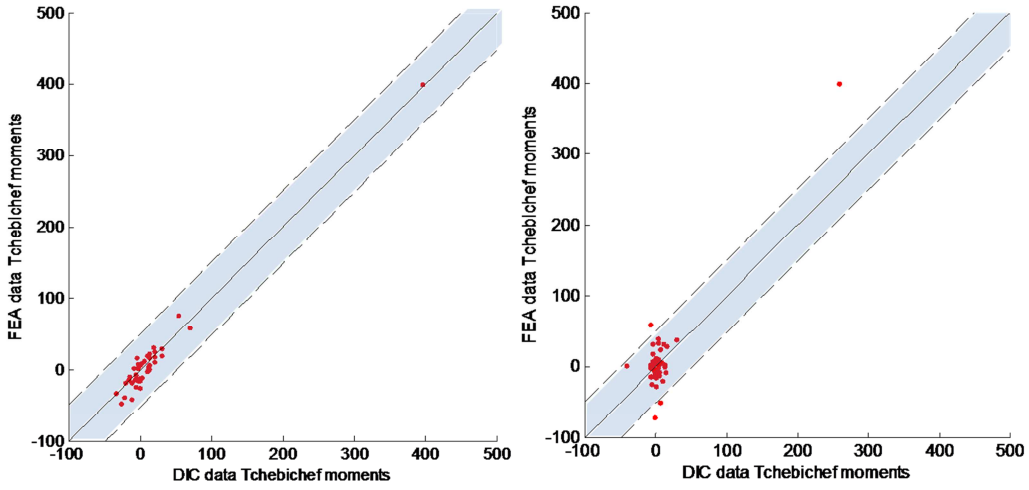

Figure A-1: Shape descriptors representing a data field from a model plotted as a function of the shape descriptors representing the corresponding data field from the validation experiment for an acceptable (left) and unacceptable (right) validation, based on whether or not the plotted points (red circles) fall within a region (green shading) defined by $s_M = s_E \pm 2u(s_E)$

This process of comparison should be repeated for each loading case for which the fundamental mechanics of the model are changed, e.g. when moving from a linear to non-linear regime, or when the boundary conditions are changed. Consideration should be given to defining an envelope for which the validation holds.

Calibration requirements

There will be uncertainties associated with all data acquired from experiments which will arise from a number of sources. An appropriate calibration procedure will permit the evaluation of the minimum measurement uncertainty that can be achieved with a particular experimental set-up, which is equivalent to the uncertainty in the calibration. A set of guidelines are available for the calibration of optical systems for strain / displacement measurement within a framework that allows traceability to be established to the international standard for length.

It is recommended that the outputs reported from a calibration should be:

(a) the calibration factor or calibration curve relating the instrument output to the strain value of the reference material. Note that the calibration should be performed for the component of strain / displacement that it is intended to use in the validation process.

(b) the field of deviations between the predicted and measured values of strain / displacement, in the Reference Material, $d(i,j)$ over the gauge area for each point (i,j)

$$d(i,j) = \left(\varepsilon\left(x_i, y_j\right)\right)_{predicted} - \left(\varepsilon\left(x_i, y_j\right)\right)_{measured} \quad \text{(A5)}$$

for the appropriate load.

(c) the calibration uncertainty, $u_{cal}(\varepsilon)$ which can be evaluated as

$$u_{cal}(\varepsilon) = \sqrt{u^2(d) + u_{RM}^2(\varepsilon)} \quad \text{(A6)}$$

where $u_{RM}(\varepsilon)$ is the reference material uncertainty and will have a number of components associated with its material properties, and the accuracy of manufacture amongst other factors. $u(d)$ is the uncertainty associated with the measurements made of the strain / displacement in the Reference Material and is calculated from the field of deviations, Eq. (A5).More details about calibration requirements may be found in [16].

[16]Guidelines for the Calibration & Evaluation of Optical Systems for Strain Measurement, www.opticalstrain.org, ISBN 978-0-9842142-2-8, 2010

Appendix II – Nomenclature

$d(i,j)$	field of deviations between predicted and measured values
(i, j)	co-ordinates of general point in image
$I(i, j)$	strain / displacement value in imagepoint (i, j)
$\hat{I}(i, j)$	Reconstruction of $I(i, j)$
k	index of coefficients, s
N	number of coefficients in feature vectors
s_k	coefficients of polynomials used for shape description
s_E, s_M	feature vector describing data from Experiment & Model
$T(i, j)$	Tchebichef polynomials
u, u_E, u_M	average reconstruction residual, defined by equation (A3), for the Experiment and Model
$u_{cal}(\varepsilon)$	Calibration uncertainty, defined in equation (A6)
$u(d)$	Uncertainty associated with measurements in the Reference Material
$u_{model}(\varepsilon)$	Uncertainty in the model
$u_{RM}(\varepsilon)$	Reference material uncertainty
$u(s_k)$	Uncertainty of shape descriptors
$u(s_E)$, $u(s_M)$	Uncertainty in feature vectors from Experiment and Model
$\varepsilon(x_i,y_i)$	strain / displacement atpoint (x_i,y_j)